A COMPACT CYLINDRICAL-SHAPE MICROSTRIP STRUCTURE WITH CLOAKING PROPERTIES FOR MUTUAL COUPLING REDUCTION IN ARRAY ANTENNAS

A Dissertation
Submitted to the Graduate Faculty
of the
North Dakota State University
of Agriculture and Applied Science

By

Syed Aftab Naqvi

In Partial Fulfillment of the Requirements
for the Degree of
DOCTOR OF PHILOSOPHY

Major Department:
Electrical and Computer Engineering

November 2014

Fargo, North Dakota

North Dakota State University
Graduate School

Title

A Compact Cylindrical-Shape Microstrip Structure With Cloaking Properties For Mutual Coupling Reduction In Array Antennas

By

Syed Aftab Naqvi

The Supervisory Committee certifies that this ***disquisition*** complies with North Dakota State University's regulations and meets the accepted standards for the degree of

DOCTOR OF PHILOSOPHY

SUPERVISORY COMMITTEE:

Dr. Benjamin D. Braaten
Chair

Dr. David A. Rogers

Dr. Ivan T. Lima

Dr. Mijia Yang

Approved:

11/19/2014
Date

Dr. Scott C. Smith
Department Chair

ABSTRACT

A cylindrical-shaped microstrip structure with cloaking properties is presented as a shielding device to reduce the mutual coupling between two patch antennas. The surface is composed of a number of 2-port microstrip (2-PM) elements printed on individual substrates and, to enclose a particular region, several 2-PM elements are interconnected into a cylindrical shape. Each 2-PM element has the capability of coupling an incident EM field on the surface to the adjacent interconnected elements. Then, because the 2-PM elements are connected into a cylindrical shape, the incident EM field is re-radiated from the other interconnected 2-PM elements in a direction away from the transmitter, achieving a behavior similar to a cloak. The prototypes in this dissertation illustrates that this surface has the additional benefit of overcoming many of the manufacturing difficulties of traditional cloaks because microstrip structures are used. To demonstrate this concept, a cylindrical surface operating at 3.89 GHz and a frequency reconfigurable surface (consisting of 2-port frequency reconfigurable microstrip elements (2-PFRM)) operating at 3.68 GHz and 3.89 GHz is simulated in HFSS and then manufactured and measured in a full anechoic chamber. Moreover, as an application, the cylindrical surface operating at 3.89 GHz is used to reduce the mutual coupling between two patch antennas operating simultaneously at 3.89 GHz. The radiation pattern and the gain of a two-element array was measured to demonstrate the negligible effects of a cylindrical surface on the far field antenna array parameters. Simulation and measurement results are in good agreement and validate the proposed EM cloak-based surface for applications

such as antenna array shielding, radar cross section (RCS) and communications in complex wireless EM environments.

ACKNOWLEDGMENTS

All the praise and thanks to almighty ALLAH and Aima tahireen (A.S) who bestowed with countless realized and unrealized blessings. There are numerous factors after every breakthrough in ones life. I would like to take this opportunity to thank each and every one of them.

I would like to thank Dr. Benjamin D. Braaten, Dr. David A. Rogers, Dr. Ivan T. Lima and Dr. Mijia Yang for serving on my PhD committee. Dr. Benjamin D. Braaten supervised me with full dedication, keen devotion and immense commitment. Humanity is the first and foremost ingredient for a teacher and I found him a best teacher. I learnt appreciation and acknowledgement for the students, besides other teaching techniques from him. I found him a researcher by nature whose research spans from electromagnetics to cars and fishing. I learnt patience and dedication as a researcher from him. I appreciate his moral support during times of my family problem. Dr. David A. Rogers is another person who inspired me as a teacher. I learned how to respond to a problem regarding the students from him. I would like to thank Dr. Ivan T. Lima and Dr. Mijia Yang for the valuable technical advices, as committee members, that helped me to clarify my research topic. I would like to thank Dr. Qaisar Abbas Naqvi who encouraged and prepared me for higher studies.

I appreciate the prayers, hard work, support, encouragement, understanding and love of my parents and brothers who never demand any responsibility instead give me time and appreciation for my endeavors. I am really grateful to all of you. Next, I would like to thank my wife who always understand, love and keep step with me in every hard time. Thank you. And all of my love for cutest, sweetest and dearest daughter Fatima, love you.

Finally, I would like to thank all of my relatives, friends and well-wishers for keeping me in your prayers and wishes all the time.

DEDICATION

To my family.

TABLE OF CONTENTS

LIST OF TABLES

LIST OF FIGURES

CHAPTER 1. INTRODUCTION

1.1. Introduction to the Electromagnetic Cloak

Following the idea of water flowing around a stone, an electromagnetic (EM) cloak bends and guides incoming waves smoothly around a cloaked region, so that the fields after having emerged from the cloak are the same as if the incident waves had just passed through free space. To outside observers, it looks as if the cloaked object was invisible [1],[2], as shown in Fig. 1. That is why, initially cloaking finds its application to hide something from EM waves. Recently, research on EM cloaks that control propagating waves has received considerable attention. This is because there are many promising benefits of using an EM cloak in the design of, for example, radar systems and phased-array antennas.

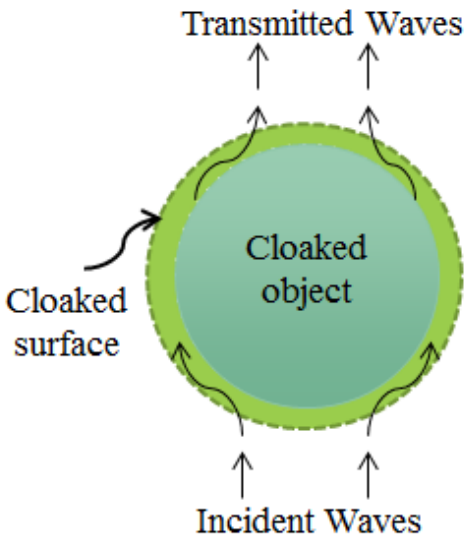

Figure 1. Top view of a cloak.

Transformation-based cloaks (TBCs) were among the first reported EM cloaks [3] - [15] as shown in Fig. 2 and Fig. 3. These cloaks operated at a single frequency and were described with rigorous mathematical computations. In addition to this foundational work, a non-Euclidean broadband TBC was proposed in [16], and carpet

cloaking was reported in [17] - [24]. Meanwhile, a TBC was proposed in [25] and was based on the decoupling of the electric and magnetic fields at DC. This work was then followed with experimental validation in [26] and [27]. Conversely, a plasmonic cloak [28] - [31] and mantle cloak [32] - [35] were designed using homogeneous and isotropic materials. These cloaks work on the principle of cancelling out the dominant scattering terms in the multipole expansion of the scattered field. The plasmonic cloak was then experimentally demonstrated in a waveguide [36] and in free space for all angles of excitation [37]. In summary, the demonstrations on cloaking have been successful; however, anisotropy and manufacturing requirements are among the drawbacks for implementing a TBC.

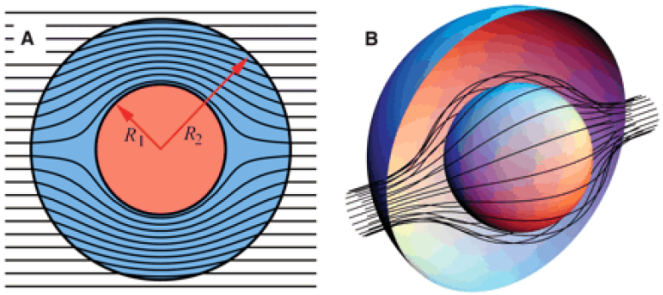

Figure 2. Principle of operation of transformation-based cloak [3].

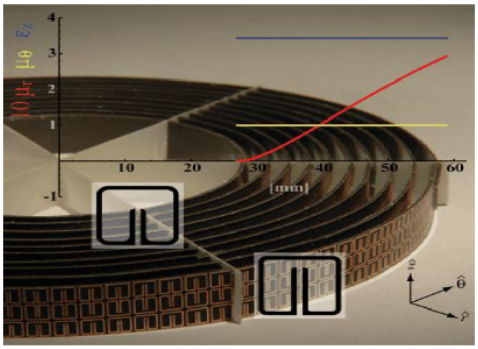

Figure 3. Experimental verification of transformation-based cloak [15].

To address some of the manufacturing difficulties with cloaking, transmission line (TL) based cloaks (or microwave network-based cloaks) have been studied as shown in Fig. 4. In TL-based cloaks, the incident wave on the structure passes

through a particular TL network [38] - [39] printed on a substrate. Recently, a TL-based cloak was reported in [40] and shown in Fig. 5. This cloak was investigated in simulations only as a new technique to reduce the reflection of an illuminated wave on a long copper cylinder. Following this work, measurements related to this cloak were then presented in [41]. Furthermore, parallel plate cloaking [42] - [44] and active cloaking using layers of components [45] - [47] are other EM cloaking techniques relating to TL-based cloaks. Overall, the research on TL-based cloaks has been progressive; however, much of the designs still require extensive manufacturing techniques and are focused only on long conducting cylinders. More research on reducing the size of these TL-based cloaks for antenna applications would be useful, as well as multi-band capabilities.

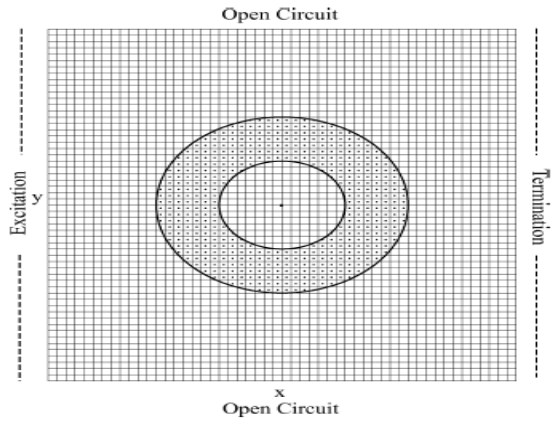

Figure 4. Principle of cloaking using transmission-line networks [39].

1.2. Application of Electromagnetic Cloaks in Antennas and Conducted Research

An EM cloak can be use to shield devices, which improves antenna performance in complex scattering and multiple-antenna environments. The applications of EM cloaks to shield an antenna's radiation and input parameters from the surrounding environment was proposed in [48] - [51]. Two dipole antennas of different sizes and operating frequencies were used to shield from one-another, so two different cloaks

operating at two different frequencies were required as shown in Fig. 6. Moreover, these applications were investigated in simulation only.

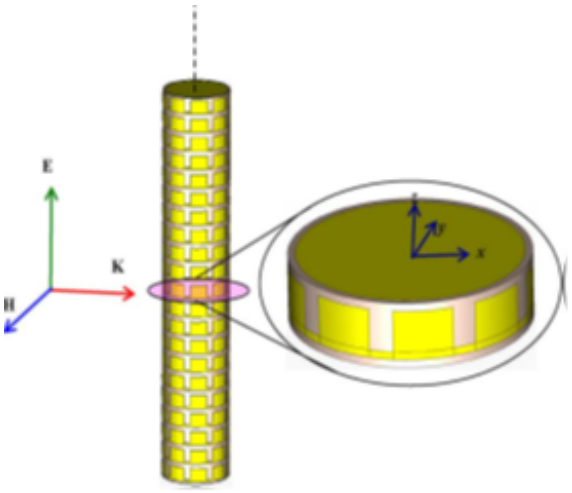

Figure 5. Long conducting cylinder enclosed by the microwave-networks based cloak [40].

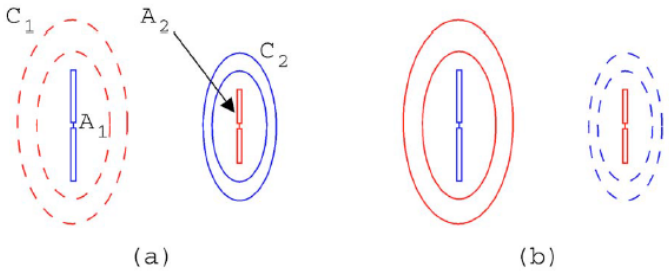

Figure 6. Radiation configuration involving antennas A_1, A_2 and cloaks C_1, C_2; (a)A_1 radiating at frequency f_1 and (b) A_2 radiating at frequency f_2. Solid boundaries for cloaks indicate perfect cloaking, whereas dashed boundaries signify that the cloak parameters assume free-space [48].

In summary, the research on EM cloaks has been progressive. However, more research on manufacturing techniques and reducing the size of these cloaks for antenna applications are required. As much of the designs focused only on long conducting cylinders and can not be use in antenna applications. Moreover, dual frequency operation of a cloak (multi-band capabilities) is another feature of interest. Thus, the objective of this dissertation is to present the surface shown in Fig. 7

(in simulation and measurement) that 1) overcomes many of the manufacturing difficulties with traditional cloaking surfaces; 2) can function at two different bands (i.e., multi-band); 3) does not operate on the principle of cloaking a large conducting cylinder, rather is small enough to be used in antenna applications; and 4) can be use as a shielding device to reduce the mutual coupling between two antennas operating simultaneously at the same frequency without affecting the far field antenna parameters (i.e., radiation pattern and gain etc.).

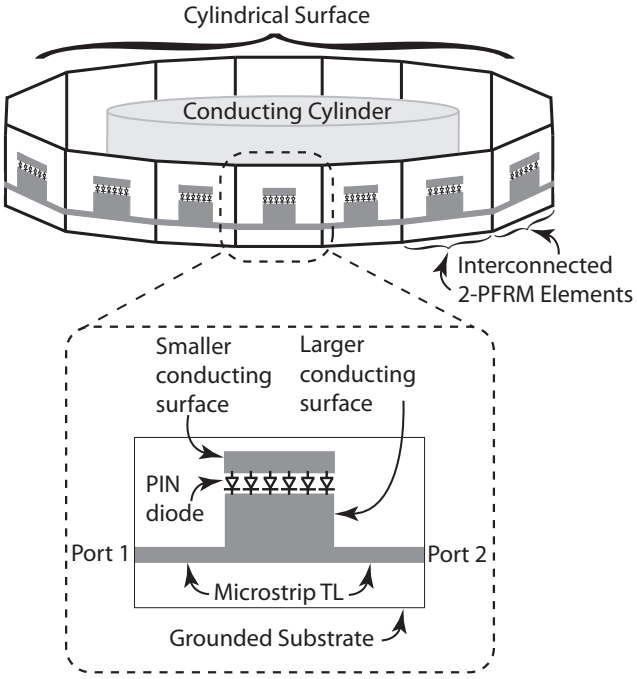

Figure 7. The proposed cylindrical surface.

CHAPTER 2. A TWO-PORT FREQUENCY RECONFIGURABLE MICROSTRIP ELEMENT FOR CYLINDRICAL-SHAPE MICROSTRIP STRUCTURE WITH CLOAKING PROPERTIES

The development of the frequency reconfigurable microstrip element shown in Fig. 7 for thin conformal cloaking surfaces is presented in this chapter. Initially, a reconfigurable microstrip element with a single-port is designed, simulated and tested. This element is then extended to a two-port reconfigurable design using the same simulation environment validated with measurements of the single-port element. The frequency reconfigurable cloaking element can be manufactured with simple microstrip printing techniques. It is shown that the two-port design is suitable for cylindrically-shaped microstrip structure with cloaking properties.

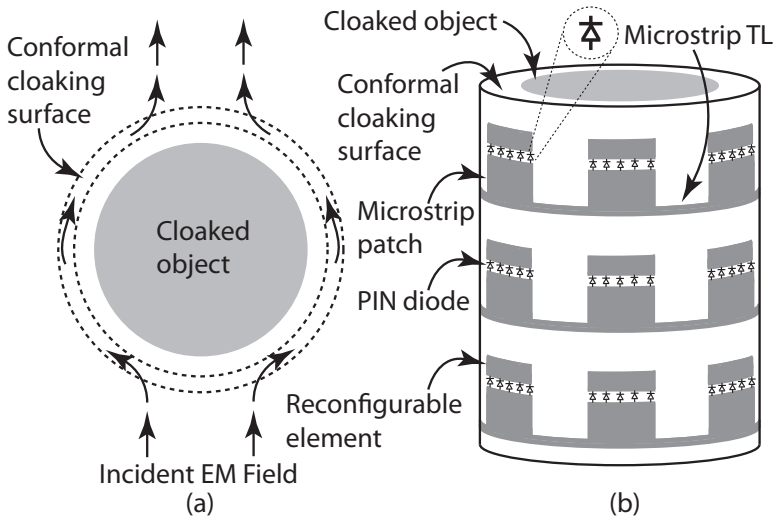

Figure 8. (a) Top-view illustration of the conformal cloak and (b) side-view of the reconfigurable microstrip cloak.

2.1. Theory and Design of the Reconfigurable Element

The key idea behind the EM cloak in this work is illustrated in Fig. 8(a). The cloaking surface is used to channel incident EM energy around an object of interest and re-radiate it in a direction different from the incident field. This is

done by developing the reconfigurable elements shown in Fig. 8(b). When an EM field is incident on the surface in Fig. 8(b), a current is induced on the microstrip patch. Then, with proper matching between elements, the current will travel down the interconnecting microstrip transmission lines (TLs) and re-radiate from other elements.

To design each element of the cloak, the one-port microstrip structure shown in Fig. 9(a) was modeled in ADS [52] and HFSS [53], manufactured and tested. Then, the two-port structure shown in Fig. 9(c) was considered and modeled in HFSS. In HFSS, ports 1 and 2 represent the interconnected elements and port 3 represents the incident field.

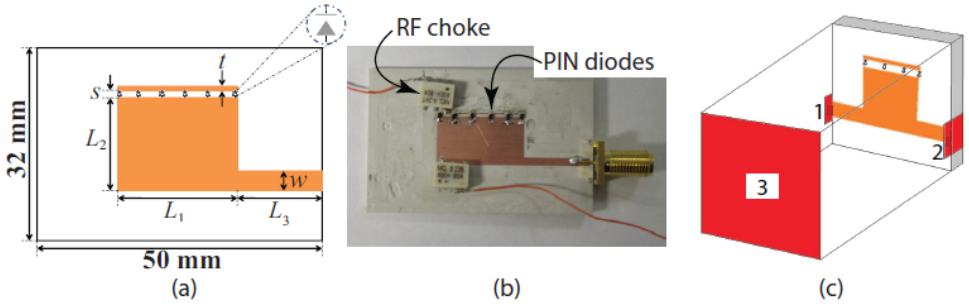

Figure 9. (a) Single-port element geometry and (b) manufactured prototype for testing ($L_1 = 20$ mm, $L_2 = 11$ mm, $L_3 = 15$ mm, $w = 1.92$ mm, $s = 0.5$ mm, $t = 0.5$ mm and the PIN diodes were manufactured by Skyworks [54] with part number: SMP1322) and (c) two-port reconfigurable cloaking array element model in HFSS.

The one- and two-port networks will be considered from an S-parameters point of view. Since the third port in Fig. 9(c) represents the incident field, and a reflection is not desired at this port, the value of S_{33} should approach $-\infty$ dB or $S_{33} \to -\infty$ dB. Then, to allow current to flow to other elements, $S_{31} = S_{12} = S_{23} = 0$ dB and $S_{11} = S_{22} \to -\infty$ dB. Furthermore, since the element is reconfigurable, these conditions are to be met at both frequency bands.

2.2. Simulation and Measurement Results

2.2.1. The single-port element

The reconfigurable single-port element was evaluated first because it could be measured and used to validate the simulation environment. The element in Fig. 9(a) was designed on a grounded $h = 1.901$ mm thick TMM10I ($\epsilon_r = 9.9, \tan\delta = .002$) substrate [55] for switching frequencies of 3.6 GHz and 4.55 GHz in both ADS and HFSS. The dimensions of the element are shown in the caption of Fig. 9 and the PIN diodes were approximately modeled as printed conductors.

The length of the microstrip patch conductor can be determined by using equation (2.1) from the wavelength of reconfigurable frequencies of interest [56].

$$L_2 = \frac{v_0}{2f\sqrt{\epsilon_{reff}}} - 2\Delta L \tag{2.1}$$

where

$$\epsilon_{reff} = \frac{\epsilon_r + 1}{2} + \frac{\epsilon_r - 1}{2}\left[1 + 12\frac{h}{L_1}\right]^{-1/2} \tag{2.2}$$

and

$$\frac{\Delta L}{h} = 0.412\frac{(\epsilon_{reff} + 0.3)\left(\frac{L_1}{h} + 0.264\right)}{(\epsilon_{reff} + 0.258)\left(\frac{L_1}{h} + 0.8\right)} \tag{2.3}$$

where v_0 is the velocity of light in free space, f is the frequency of operation, L_1 is width of the microstrip patch conductor and ΔL is the electrical increment in length of the patch because of the fringing effects.

To verify the simulations, the manufactured element in Fig. 9(b) was measured and the results are shown to agree in Fig. 10. Notice that in both cases, the element resonates at two frequencies i.e., for the diodes off case, at 3.89 GHz and 4.62 GHz

while for the diodes on case, at 3.68 GHz and 4.49 GHz. It will be shown in the next section, that the condition where $S_{33} \rightarrow -\infty$ dB is only satisfied in the switching bands.

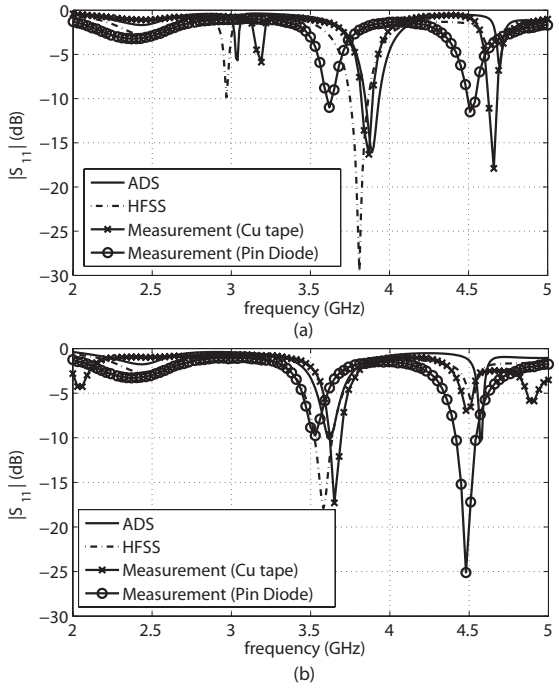

Figure 10. S_{11} for reconfigurable single-port element when Pin Diodes are (a) OFF and (b) ON (Cu tape is modeled equivalent to pin diodes in simulations so measurements using Cu tape are necessary to agree with simulations).

2.2.2. The two-port element

Next, the two-port element in Fig. 9(c) was simulated in HFSS, except for this design a TL was added to the opposite side of the reconfigurable patch (for symmetry) and a third-port was defined in the simulator to represent an incident EM field. The dimensions of the TLs were the same as the values in Fig. 9(b). The HFSS simulations results are shown in Fig. 11. Again, the diodes were approximated as printed conductors in HFSS [57]. The results in Fig. 11(a) show a low reflection at port 3 at the 3.68 GHz and 3.89 GHz bands and nothing at at 4.49 GHz and 4.62 GHz as was in case of single-port element, indicating a frequency reconfigurable cloaking element. Furthermore, Fig. 11(b) shows that the coupling capability between

elements of the proposed design has been improved by −10 dB as compared to the super thin cloaks presented in [40]; which shows an improvement in the element for both bands.

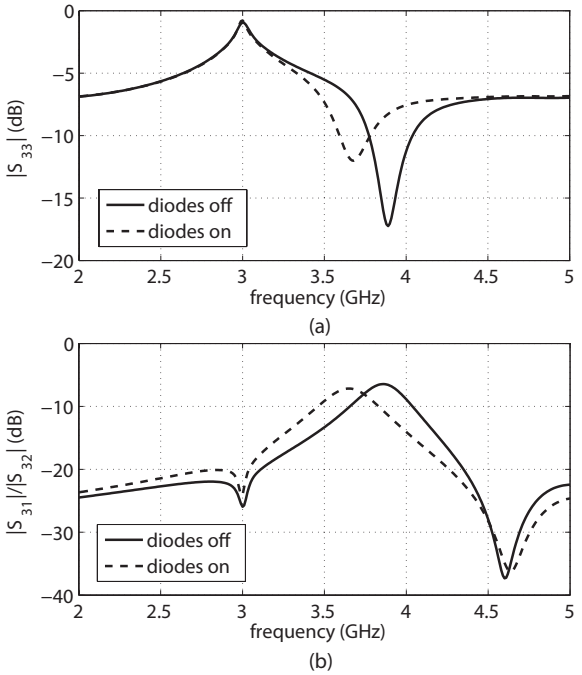

Figure 11. (a) S_{33} and (b) S_{31}/S_{32} for the three port reconfigurable cloaking array element.

2.3. Discussion

The single-port results in Fig. 10 show different switching frequencies than the results in Fig. 11. This is thought to be due to the extra TL added to the other side of the reconfigurable patch in Fig. 9(c). Furthermore, a good match was achieved with the single-port structure; however, the radiation properties of the patch may not be significant enough for cloaking surface.

In summary, a frequency reconfigurable element for a thin cylindrical-surface with cloaking properties was investigated in this chapter. Initially, a single-port microstrip structure with PIN diodes was designed and presented. Then, this single-port element was used to develop a two-port element suitable for cloaking on conformal surfaces. Overall, simulations were validated with measurements, and

it was shown that a reconfigurable microstrip element for cylindrical-shape surface with cloaking properties could be designed.

CHAPTER 3. A COMPACT FREQUENCY RECONFIGURABLE CYLINDRICALLY-SHAPED MICROSTRIP STRUCTURE WITH CLOAKING PROPERTIES

A frequency reconfigurable cylindrical shaped surface with the characteristics of an EM cloak is presented in this chapter. The surface is composed of a number of 2-port frequency reconfigurable microstrip (2-PFRM) elements printed on individual substrates and, to enclose a particular region, several 2-PFRM elements are interconnected into a cylindrical shape (as shown in Fig. 12). Each 2-PFRM element has the capability of coupling an incident EM field on the surface to the adjacent interconnected elements. Then, because the 2-PFRM elements are connected in to a cylindrical shape, the incident EM field is re-radiated from the other interconnected 2-PFRM elements in a direction away from the transmitter, achieving a behavior similar to a cloak. Moreover, to demonstrate this concept, a frequency reconfigurable surface operating at 3.68 GHz and 3.89 GHz is simulated in HFSS, manufactured and measured in a full anechoic chamber. The prototype in this chapter illustrates that this surface has the additional benefit of overcoming many of the manufacturing difficulties of traditional cloaks because microstrip structures are used. Simulation and measurement results are in good agreement and validate the proposed EM cloak-based surface for applications such as antenna array shielding to reduce mutual coupling, radar cross section reduction and communications in complex electromagnetic environments.

3.1. Principle of Operation and Design

The frequency reconfigurable surface shown in Fig. 12 is presented and addresses the cylindrical-shape microstrip structure with cloaking properties. This surface consists of the 2-port frequency reconfigurable microstrip (2-PFRM) elements shown

in Fig. 12 (inset) interconnected in a cylindrical manner. The conductors are printed on a grounded substrate with port 1 and port 2 on two sides connected together with a printed microstrip TL. Each 2-PFRM element also has a larger conducting surface connected to the TL and this surface is used to couple the incident EM wave on the substrate surface to ports 1 and 2 at the higher reconfigurable frequency of operation. Also connected to this larger surface are six (6) PIN diodes and a smaller conducting surface. By biasing the PIN diodes simultaneously on each element, the overall length of the conducting surface is enlarged, which then moves the operation of the cylindrical surface to the lower reconfigurable frequency of operation.

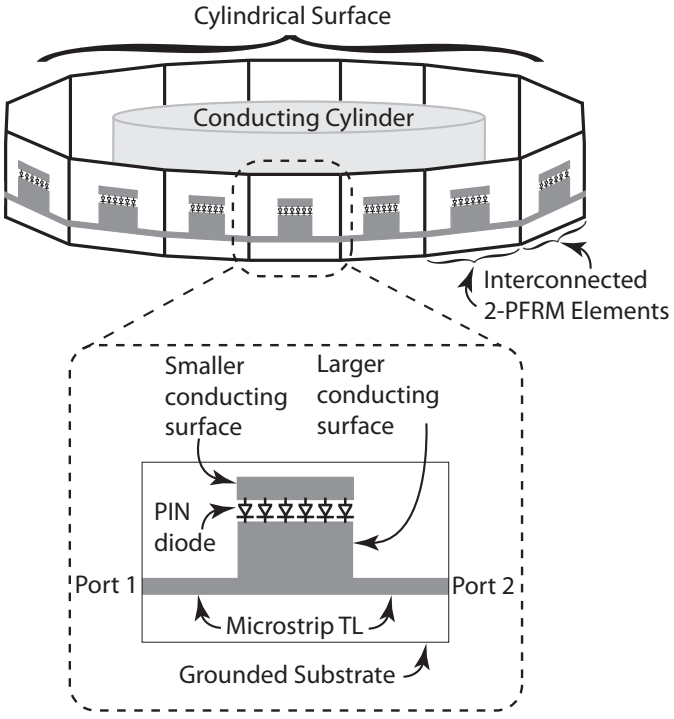

Figure 12. Illustration of the cylindrical-shaped surface with interconnected 2-port frequency reconfigurable microstrip (2-PFRM) elements and (inset) a zoomed in drawing of each 2-PRFRM element.

3.2. The 2-PFRM Element

For illustration on the behavior of the 2-PFRM element, consider the drawing in Fig. 13. This geometry was used to simulate each individual 2-PFRM element in

HFSS. Also, to represent an incident EM field (i.e., illuminating wave) on the surface of the substrate, port 3 was defined (shown in green) [40] in addition to ports 1 and 2. This then allows a designer to directly compute the S-parameters of the three-port network in HFSS and determine how well the incident field is coupled from port 3 to ports 1 and 2 in both frequency reconfigurable bands (i.e., by computing S_{13} and S_{23}). Finally, the length of the larger and smaller printed conductors can be determined from the wavelength of reconfigurable frequencies of interest.

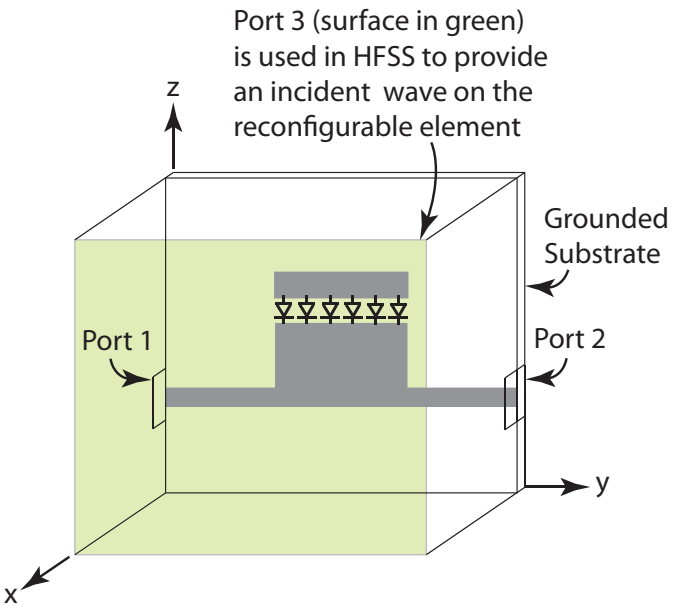

Figure 13. Illustration of the 2-PFRM element being simulated in HFSS. The third port is added to the design to represent an incident field on the surface of the substrate.

Overall, in terms of S-parameters for the simulation set-up in Fig. 13, the following properties are of interest: 1) $S_{33} \rightarrow -\infty$ dB, indicating that minimal reflection is occurring at port 3 and hence not off of the element in the direction back towards the source; 2) $S_{13} = S_{23}$ = -3.0 dB which means that much of the incident power on port 3 is coupled symmetrically to ports 1 and 2; and finally 3) $S_{11} = S_{22} \rightarrow$ -∞ dB, indicating minimal reflection of the power between adjacent 2-PFRM elements. Furthermore, these conditions are to be met for both frequency reconfigurable bands of operation. After extensive HFSS simulations, the S-parameter

results were determined for the two frequency reconfigurable values of $f_1 = 3.68$ GHz and $f_2 = 3.89$ GHz and were reported in [41]. The design shown in Fig. 14 was simulated on a Rogers TMM10I substrate ($\varepsilon_r = 9.9$ and $\tan\delta = 0.002$) with a thickness of 1.901 mm. In summary, $|S_{33}|$ was equal to -12 dB and -17.2 dB at 3.68 GHz and 3.89 GHz, respectively. Furthermore, $|S_{31}|$ was equal to -7.2 dB and -6.5 dB at 3.68 GHz and 3.89 GHz, respectively.

3.3. Simulation in HFSS of the Reconfigurable Cylindrical Surface and Validation with Measurements

Next, ten (10) of the 2-PFRM elements presented in Fig. 14 were interconnected in HFSS and simulated here on the same 1.901 mm thick TMM10I Rogers substrate for the first time. This then resulted in the new overall geometry presented in Fig. 12. However, instead of using PIN diodes and RF chokes, copper tape was put in place to represent a biased diode and the copper tape was then removed to represent an unbiased diode. It has been shown in [57] that copper tape is a fairly accurate model for biased PIN diodes. The radius of the cylindrical surface was 7.9 cm, which is $0.96\lambda_1$ and $1.02\lambda_2$ at 3.68 GHz and 3.89 GHz, respectively, and $\lambda_{1,2} = c/f_{1,2}$.

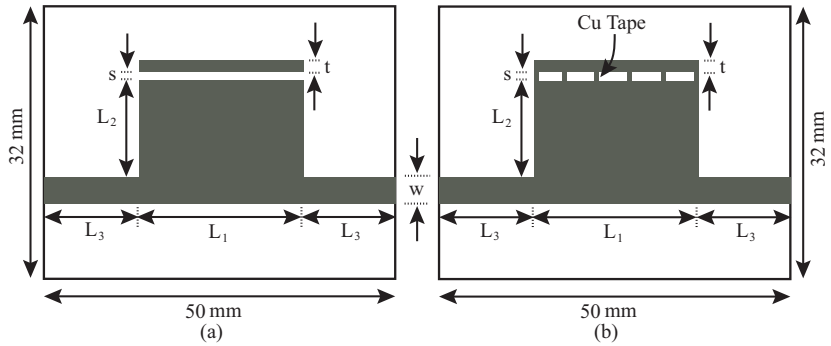

Figure 14. The two port frequency reconfigurable element (a) without copper tape to represent an unbiased PIN diode and (b) with copper tape to represent a biased PIN diode ($L_1 = 20.0$ mm, $L_2 = 11.0$ mm, $L_3 = 15.0$ mm, $w = 1.92$ mm, $s = 0.5$ mm, $t = 0.5$ mm).

To determine whether or not the reconfigurable cylindrical surface was reducing the scattered wave in the direction back towards the transmitting antenna, the

problem shown in Fig. 15(a) was simulated in HFSS first. This problem consisted of two microstrip patches with center frequencies at $f_1 = 3.68$ GHz separated by a distance of $4\lambda_1$. In other words, the separation between the microstrip antennas was kept at four (4) wavelengths apart for both reconfigurable frequencies of operation. This step was taken first to establish the HFSS simulation environment. Next, for validation, the microstrip patch antennas were manufactured, placed in a full-anechoic chamber with the same orientation as the HFSS simulation (as shown in Fig. 15(b)) and the S-parameters were measured. The simulated results are shown to agree with the S_{12} measurements in Fig. 16(a). These results indicate that the HFSS simulation and measurement environment are similar and the scattering effects of a compact conducting cylindrical surface can now be explored.

Next, a copper cylinder with a fixed radius of 7.5 cm and a fixed height of 3.2 cm was defined between the two patch antennas (as shown in Fig. 15(c)). The cylinder was centered between the two patches and the S_{12} values were again simulated in HFSS. For validation then a copper cylinder with the same dimensions was manufactured and placed between the two patch antennas in the full anechoic chamber (as shown in Fig. 15(d)). The measured S_{12} values from this experiment are shown to agree with simulations in Fig. 16(b) for 3.68 GHz. Comparing the values in Fig. 16(a) to Fig. 16(b) shows that $|S_{12}|$ is 11 dB lower with the cylinder in place; which provides a metric for determining whether or not the reconfigurable cylindrical surface has the behavior similar to a cloaking structure.

Then, the cylindrical surface with the 10 2-PFRM elements presented in Fig. 14 was simulated in HFSS (Fig. 15(e)), manufactured and tested in the full anechoic chamber (Fig. 21(f)). These results are shown in Fig. 16(c) for 3.68 GHz.

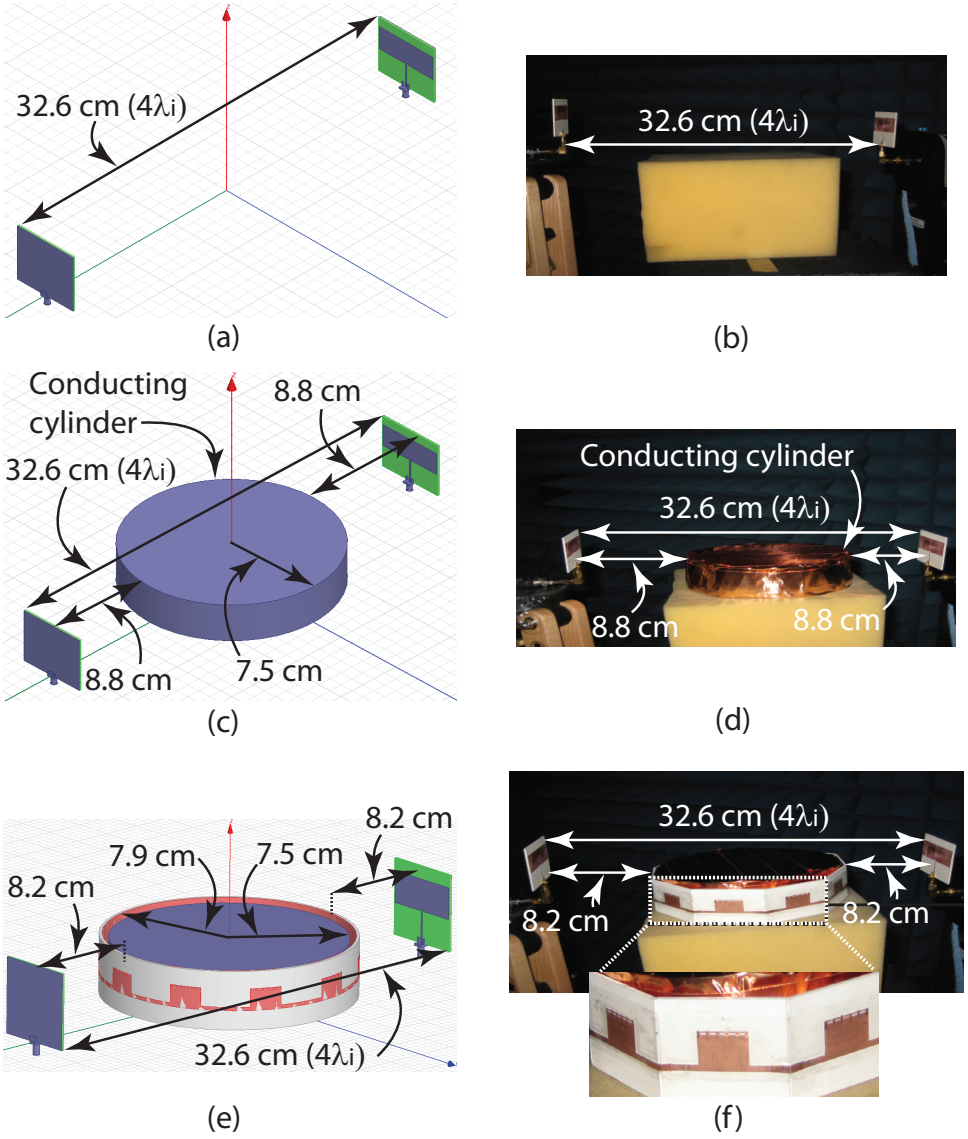

Figure 15. For $i = 1$, (a) HFSS simulation geometry of the two microstrip antennas without the conducing cylinder and reconfigurable cylindrical surface at 3.68 GHz; (b) measurement set-up of the two microstrip antennas without the conducing cylinder and reconfigurable cylindrical surface at 3.68 GHz; (c) HFSS simulation geometry of the two microstrip antennas with the conducing cylinder in the middle and no reconfigurable cylindrical surface at 3.68 GHz; (d) measurement set-up of the two microstrip antennas with the conducing cylinder in the middle and no reconfigurable cylindrical surface at 3.68 GHz in the full anechoic chamber; (e) HFSS simulation geometry with both the conducing cylinder and reconfigurable cylindrical surface between the two microstrip patch antennas at 3.68 GHz and (f) measurement set-up in the full anechoic chamber of the two microstrip antennas, and the conducing cylinder and reconfigurable cylindrical surface prototype in the middle at 3.68 GHz.

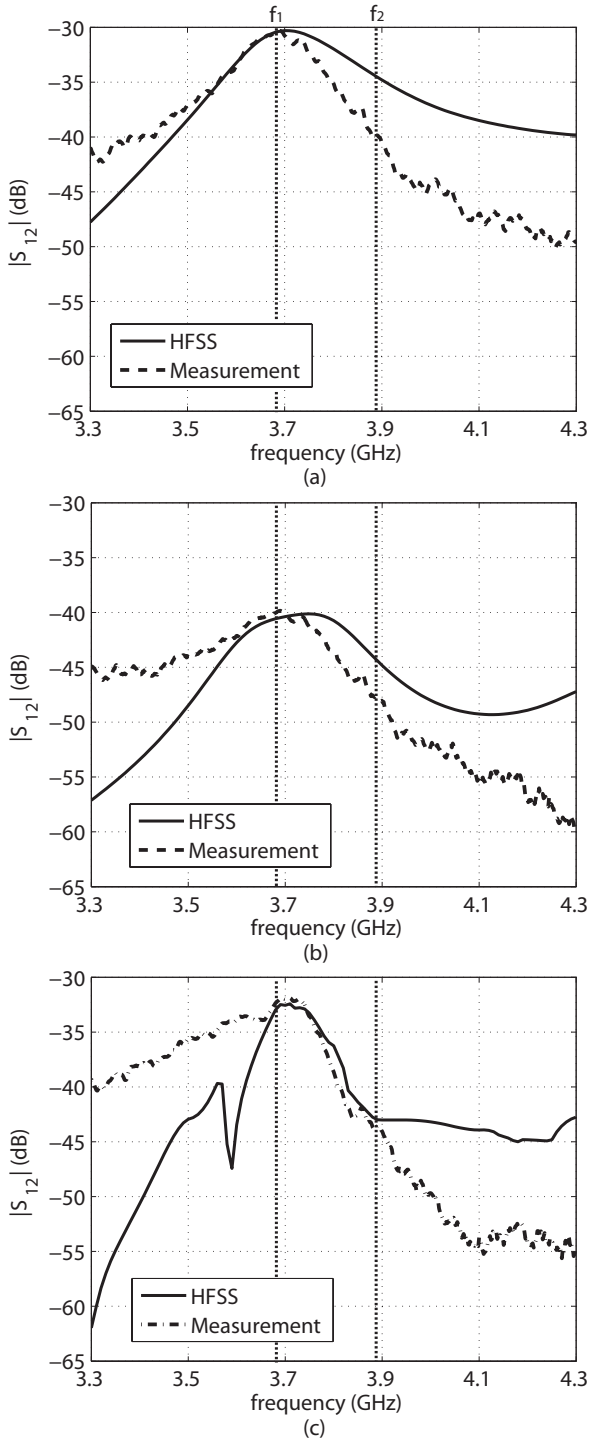

Figure 16. Measured and simulated S_{12} values for (a) the two 3.68 GHz patch antennas without the conducting cylinder and reconfigurable cylinder in place (b) the two patch antennas operating at 3.68 GHz and only the conducting cylinder in between the elements to provide scattering and (c) the two patch antennas with the conducting cylinder surrounded by the reconfigurable cylindrical surface at 3.68 GHz.

Finally, to illustrate the reconfigurability of the cylindrical surface, a second prototype was manufactured with the copper connections representing the PIN diodes removed. This then reconfigures the surface to operate at 3.89 GHz. The exact same procedure for simulating and measuring the surface at 3.68 GHz was repeated here for 3.89 GHz except 1) $\lambda_i = \lambda_2$ $(i = 2)$ to keep the same electrical spacing between the patch antennas at both reconfigurable frequencies, as shown in Fig. 17(a); 2) the spacing between the copper cylinder and the patch antennas was changed to 7.9 cm as shown in Fig. 17(c); and 3) the spacing between the patch antennas and the reconfigurable cylindrical surface was changed from 8.2 cm to 7.3 cm as shown in Fig. 17(e). The results from these simulations and measurements are shown in Fig. 18(a) - (c).

3.4. Discussion

The results in Figs. 16 and 18 show that the $|S_{12}|$ values between the patch antennas without the conducting cylinder in place are measured (simulated) to be -30.5 dB (-30.3 dB) and -30.5 dB (-30.8 dB) at 3.68 GHz and 3.89 GHz, respectively. Then, with the conducting cylinder in place between the patches, the $|S_{12}|$ values were measured (simulated) to be -40.0 dB (-40.6 dB) and -40.5 dB (-41.0 dB) at 3.68 GHz and 3.89 GHz, respectively. Next, when the frequency reconfigurable cylindrical surface was placed around the conducting cylinder, the measured (simulated) $|S_{12}|$ values were determined to be -31.8 dB (-32.5 dB) and -31.7 dB (-31.8 dB) at 3.68 GHz and 3.89 GHz, respectively. This illustrates that the cylindrical surface is demonstrating a behavior similar to a cloak because the $|S_{12}|$ values of the patch antennas with the cylinder and reconfigurable cylindrical surface are within 1.3 dB of the $|S_{12}|$ values of the patch antennas without the conducting cylinder in place (i.e., without a surface to cause a reflection between the patch antennas).

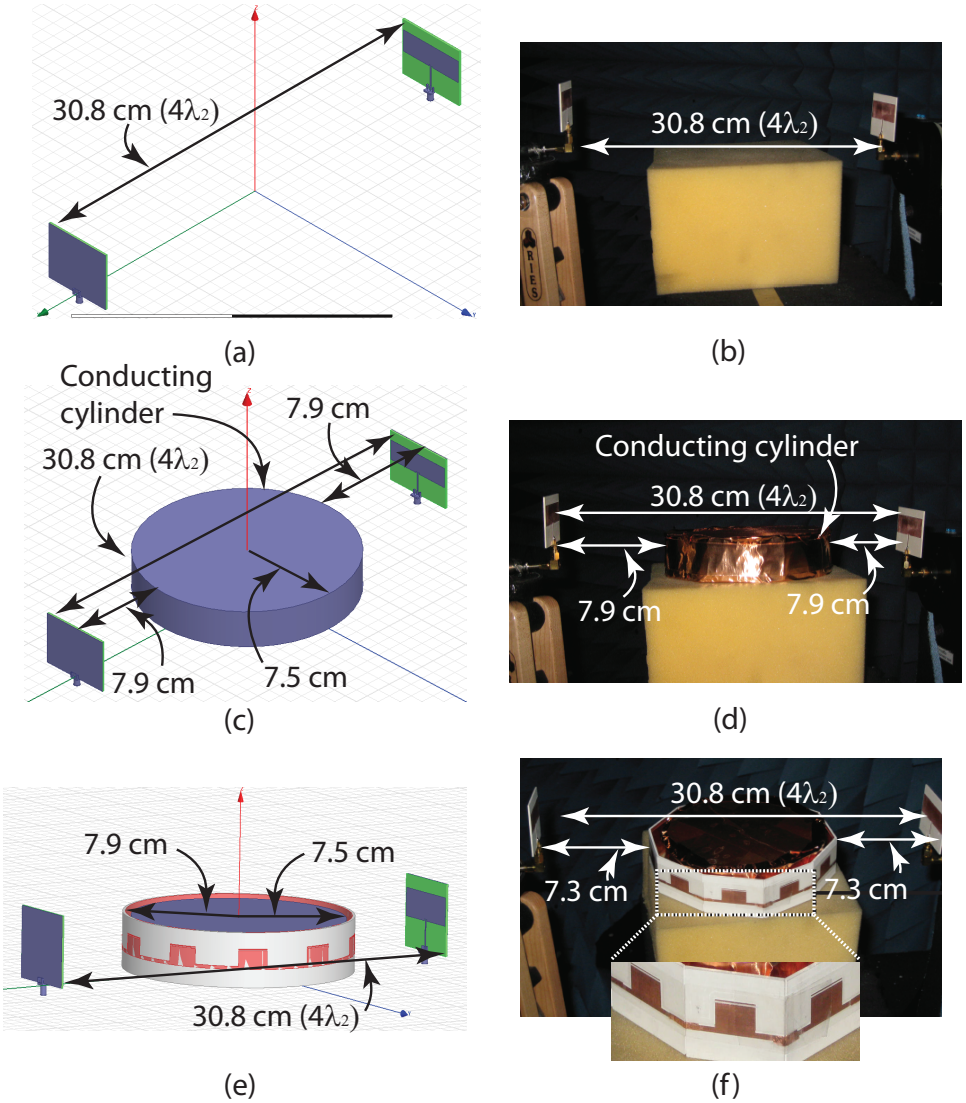

Figure 17. (a) HFSS simulation geometry of the two microstrip antennas without the conducing cylinder and reconfigurable cylindrical surface at 3.89 GHz; (b) measurement set-up of the two microstrip antennas without the conducing cylinder and cylindrical surface at 3.89 GHz in the full anechoic chamber; (c) HFSS simulation geometry of the two microstrip antennas with the conducing cylinder in the middle and no reconfigurable cylindrical surface at 3.89 GHz; (d) measurement set-up of the two microstrip antennas with the conducing cylinder in the middle and no cylindrical surface at 3.89 GHz in the full anechoic chamber; (e) HFSS simulation geometry with both the conducing cylinder and reconfigurable cylindrical surface between the two microstrip patch antennas at 3.89 GHz and (f) measurement set-up in the full anechoic chamber of the two microstrip antennas, and the conducing cylinder and reconfigurable cylindrical surface prototype in the middle at 3.89 GHz.

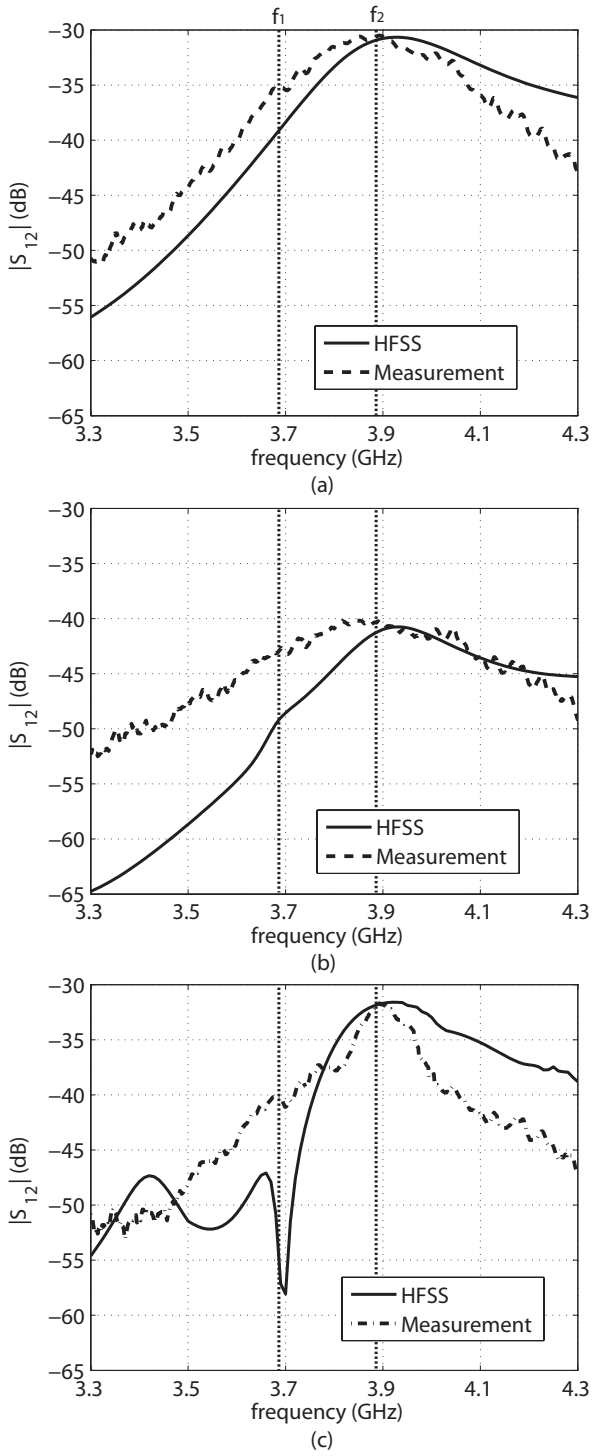

Figure 18. Measured and simulated S_{12} values for (a) the two 3.89 GHz patch antennas without the conducting cylinder and reconfigurable cylinder in place (b) the two patch antennas operating at 3.89 GHz and only the conducting cylinder in between the elements to provide scattering and (c) the two patch antennas with the conducting cylinder surrounded by the reconfigurable cylindrical surface at 3.89 GHz.

In summary, it was shown that the surface presented here is capable of reducing the scattering from a conducting cylinder in both frequency reconfigurable bands and achieving $|S_{12}|$ values within 1.3 dB of the values without the conducting cylinder in place.

CHAPTER 4. MUTUAL COUPLING REDUCTION BETWEEN TWO PATCH ANTENNAS USING CYLINDRICALLY-SHAPED MICROSTRIP STRUCTURE WITH CLOAKING PROPERTIES

A cylindrical-shaped microstrip surface with cloaking properties is presented as a shielding device to reduce the mutual coupling between two patch antennas. For the first step, the cylindrical-shaped surface in Fig. 12 operating at 3.89 GHz was simulated in HFSS and measured in an anechoic chamber to demonstrate the characteristics of an electromagnetic (EM) cloak. The surface comprises of a number of 2-port microstrip (2-PM) elements interconnected into a cylindrical shape to enclose a particular region. Each 2-PM element has the capability of coupling an incident EM filed on the surface and transmit to the adjacent interconnected element. In this way, as the 2-PM elements are connected in to a cylindrical shape, the incident EM field is re-radiated from the other interconnected 2-PM elements in a direction away from the transmitter; achieving a behavior similar to an EM cloak. Then, the second step is to use the cylindrical-shape microstrip cloaking surface as a shield to reduce the mutual coupling between the two patch antennas. Overall, simulation and measurement results are in good agreement with each other and validate the application of the proposed EM cloak-based surface for antenna array shielding to reduce the mutual coupling by 6 dB. The phenomenon can be used to improve antenna performance in multiple-antenna environments, antenna array shielding and radar cross section reduction.

4.1. Principle of Operation and Design

A compact cylindrical surface exhibiting the cloaking properties is presented as a shielding device to an enclosed antenna from the other placed outside of the surface as illustrated in Fig. 19. The cylindrical surface consists of the 2-port microstrip

(2-PM) elements shown in Fig. 19 interconnected in a cylindrical manner. Each 2-PM element has a conducting patch connected to the printed microstrip TL as shown in Fig. 20(a). Port 1 and port 2 are on opposite sides connected together with a TL. The conductors are printed on a grounded substrate. The conducting patch is used to couple the incident EM wave on the substrate surface to ports 1 and 2 at the operating frequency via the connected TL. While EM surface waves radiating from the outer antenna are illuminated on the cylindrical-surface, 2-PM elements will guide them around the enclosed antenna to re-radiate away from the outer antenna. In this way the cylindrical surface is used to reduce the mutual coupling between the two antennas radiating at the same time and frequency.

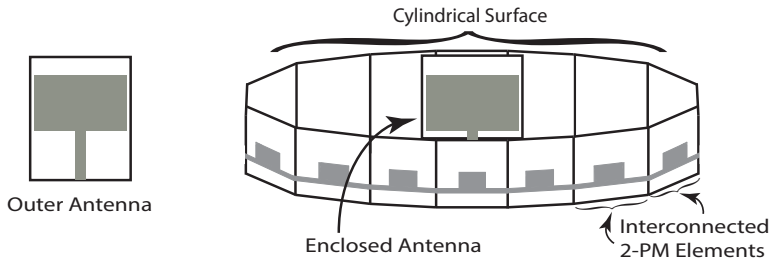

Figure 19. Illustration of the cylindrical-shaped surface with interconnected 2-port microstrip (2-PM) elements cloaked an antenna from the other, both antennas are operating simultaneously at same frequency.

4.2. The 2-port Microstrip Element

The geometry of the 2-PM element shown in Fig. 20(a) was used to simulate each individual 2-PM element in HFSS [53]. Fig. 20(b) shows a drawing of the simulation setup in HFSS. Port 3 (shown in green) was defined as the wave-port to excite the 2-PM element in addition to ports 1 and 2 [40]. The setup is helpful to directly compute the S-parameters of the three-port microwave network in HFSS. Also, this allows the designer to determine how well the illuminated field is coupled from port 3 to ports 1 and 2 (i.e., by computing S_{13} and S_{23}) at the frequency of operation. Again, the 2-PM element simulated in HFSS is required to exhibit the following S-parameters (in order to be use in a cloaking surface) at the operating

frequency: 1) $S_{33} \rightarrow -\infty$ dB, indicating minimum reflection at port 3 and allowing maximum power transfer to the surface of the 2-PM element; 2) $S_{31} = S_{32} = -3.0$ dB, indicating much of the incident power on port 3 is coupled symmetrically to port 1 and 2; and 3) $S_{11} = S_{22} \rightarrow -\infty$ dB, which shows the minimum reflection of the power (and thus maximum power flow) between adjacent 2-PM elements. The required S-parameter results were attained in HFSS simulations at 3.89 GHz and were reported in [41]. The design shown in Fig. 20(a) was simulated on a Rogers [55] TMM10I substrate ($\varepsilon_r = 9.9$ and $\tan\delta = 0.002$) with a thickness of 1.901 mm. In summary, $|S_{33}|$ was equal to -17.2 and $|S_{31}|$ was equal to -6.5 dB at 3.89 GHz.

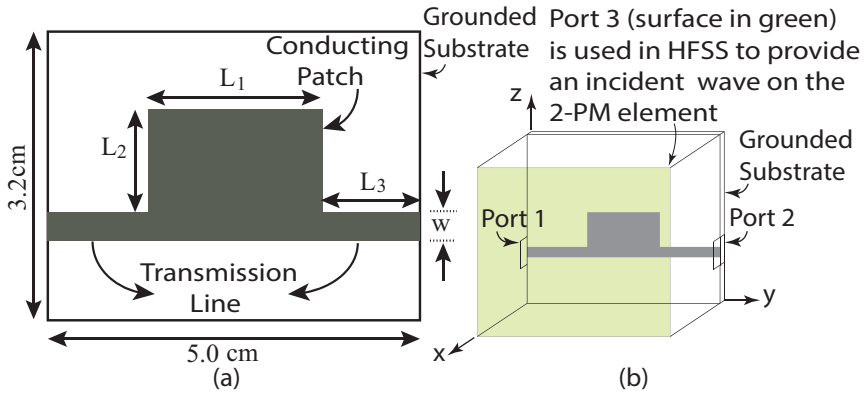

Figure 20. Geometry and simulation setup of the 2-port microstrip element in HFSS (a) The two port element ($L_1 = 2.0$ cm, $L_2 = 1.1$ cm, $L_3 = 1.5$ cm, $w = 0.192$ cm) (b) Illustration of the 2-PM element being simulated in HFSS. The third port is added to the design to represent an incident field on the surface of the substrate.

4.3. Simulation in HFSS of the Cylindrical Surface and Validation with Measurements

As with the reconfigurable surface, ten (10) of the 2-PM elements presented in Fig. 20(a) were interconnected in HFSS and simulated on the same 1.901 mm thick TMM10I Rogers substrate for the first time. This then resulted in the cylindrical surface presented in Fig. 19. The radius of the cylindrical surface was 7.9 cm, which is 1.02λ at 3.89 GHz, where $\lambda = c/f$.

In order to determine the functionality of the designed cylindrical surface, (i.e., whether or not it is supportive to minimize the reflection of illuminated EM field on the surface and direct them to the other side) the problem shown in Fig. 21(a) was simulated in HFSS first. Two microstrip patch antennas, designed at a center frequency of 3.89 GHz were separated by 4 wavelengths (4λ). This step was taken to establish the HFSS simulation environment. Next, for validation, the microstrip patch antennas were manufactured, placed in a full-anechoic chamber with the same orientation as the HFSS simulation (as shown in Fig. 21(b)) and the S-parameters were measured. The simulation and measurement results of $|S_{12}|$ or $|S_{21}|$ are shown in Fig. 22(a) and are in good agreement, which validates the simulation and measurement setups.

Next, to explore the scattering effects of a compact conducting cylindrical surface a copper cylinder of radius 7.5 cm and height 3.2 cm was defined between the two patch antennas in the HFSS simulation, as shown in Fig. 21(c). To validate, a copper cylinder with the same dimensions was manufactured and placed between the two patch antennas in a full anechoic chamber, as shown in Fig. 21(d). The copper cylinder was centered and the $|S_{12}|$ or $|S_{21}|$ values were taken and are shown in 22(b). The measured and simulated values are in good agreement and are 11 dB lower than the results in Fig. 22(a) at the operating frequency; providing a metric for determining whether or not the cylindrical surface has a behavior similar to a cloaking surface.

Finally, the copper cylinder was enclosed by the cylindrical surface consisting of the 10 2-PM elements in HFSS (Fig. 21(e)) and measured in the full anechoic chamber (Fig. 21(f)) to analyze the behavior of the designed cylindrical surface. Simulation and measurement results are shown in 22(c).

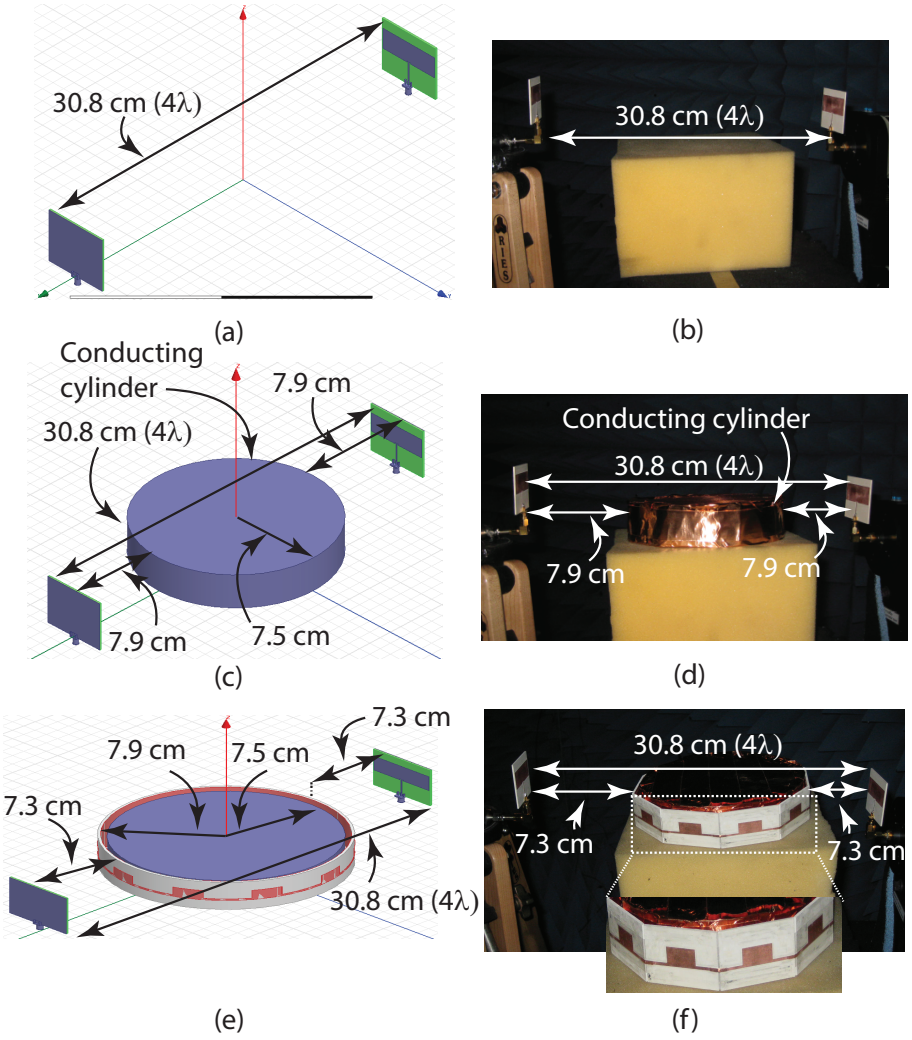

Figure 21. (a) HFSS simulation geometry of the two microstrip antennas without the conducing cylinder and cylindrical surface at 3.89 GHz; (b) measurement set-up of the two microstrip antennas without the conducing cylinder and cylindrical surface at 3.89 GHz; (c) HFSS simulation geometry of the two microstrip antennas with the conducing cylinder in the middle and no cylindrical surface at 3.89 GHz; (d) measurement set-up of the two microstrip antennas with the conducing cylinder in the middle and no cylindrical surface at 3.89 GHz in the full anechoic chamber; (e) HFSS simulation geometry with both the conducing cylinder and cylindrical surface between the two microstrip patch antennas at 3.89 GHz and (f) measurement set-up in the full anechoic chamber of the two microstrip antennas, and the conducing cylinder and cylindrical surface prototype in the middle at 3.89 GHz.

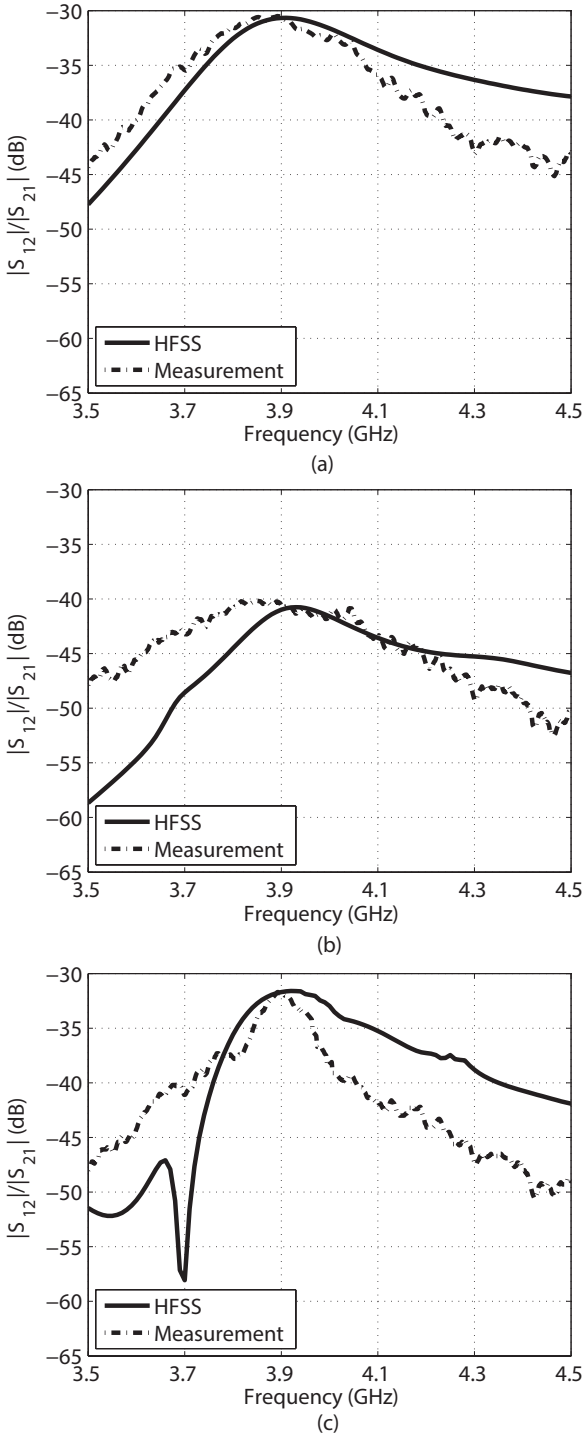

Figure 22. Measured and simulated S_{12} values for (a) the two 3.89 GHz patch antennas without the conducting cylinder and reconfigurable cylinder in place (b) the two patch antennas operating at 3.89 GHz and only the conducting cylinder in between the elements to provide scattering and (c) the two patch antennas with the conducting cylinder surrounded by the reconfigurable cylindrical surface at 3.89 GHz.

The results in Fig. 22 shows that the $|S_{12}|$ values of the patch antennas without the copper cylinder and cylindrical surface in place were simulated and measured to be $-30.8\ dB$ and $-30.5\ dB$, respectively. While with the copper cylinder in place between the patch antennas, the $|S_{12}|$ values were simulated and measured to be $-41.0\ dB$ and $-40.5\ dB$, respectively. Then, when the copper cylinder was surrounded by the cylindrical surface the $|S_{12}|$ values were simulated and measured to be $-31.8\ dB$ and $-31.7dB$, respectively. The difference between the values of $|S_{12}|$ with and without the copper cylinder surrounded by cylindrical surface are within $1.3\ dB$. Thus means, that with the presence of the cylindrical surface between the two antennas there is negligible reflection. This illustrates that the cylindrical surface is demonstrating a behavior similar to a cloak.

4.4. Mutual Coupling Reduction between Two Neighboring Patch Antennas by using the Cylindrical Surface

The prototype cylindrical surface was used next to reduce the mutual coupling between two antennas. One of the antennas was surrounded by the cylindrical surface to shield from the EM waves of another antenna. This then resulted in the overall geometry presented in Fig. 19. Two microstrip patch antennas, each radiating at 3.89 GHz, were placed side by side and simulated to obtain the S-parameters in HFSS as shown in Fig. 23(a).

Next, for validation, two of the microstrip patch antennas shown in Fig. 23(a) were printed on a grounded 1.52 mm thick TMM4 Rogers ($\varepsilon_r = 4.7$ and $\tan\delta = 0.002$) substrate [55]. Then, the microstrip patch antennas were placed in a full-anechoic chamber with the same orientation as the HFSS simulation, as shown in Fig. 23(b), and the S-parameters were measured. Next the cylindrical surface was placed around the antenna fed at port 1 (i.e. on the right), and simulated in HFSS (as shown in Fig. 24(a)). For validation then, one of the patch antennas shown in Fig. 23(b) was

enclosed by the cylindrical surface in the full anechoic chamber (as shown in Fig. 24(b)) and the S-parameters were measured.

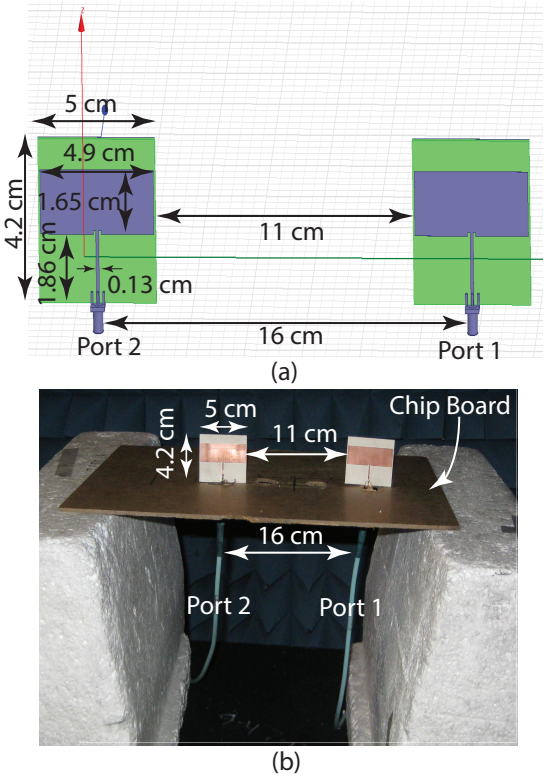

Figure 23. (a) HFSS simulation geometry of the two microstrip antennas radiating at 3.89 GHz; (b) measurement set-up of the two microstrip antennas radiating at 3.89 GHz in a full anechoic chamber.

The results in Fig. 25 shows that the $|S_{12}|$ values between the two microstrip patch antennas without the cylindrical surface in place are simulated and measured to be $-35.3\ dB$ and $-35.5\ dB$, respectively. Then, when the antenna driven with port 1 was shielded by the cylindrical surface, the simulated and measured $|S_{12}|$ values were reduced to $-42\ dB$ and $-41.5\ dB$, respectively. This illustrates that the cylindrical surface is demonstrating a behavior similar to a cloaking-surface because the difference between the $|S_{12}|$ values of the microstrip patch antennas with and without the cylindrical surface is more than 6 dB. The cylindrical surface guides the incident EM waves to shield the enclosed antenna.

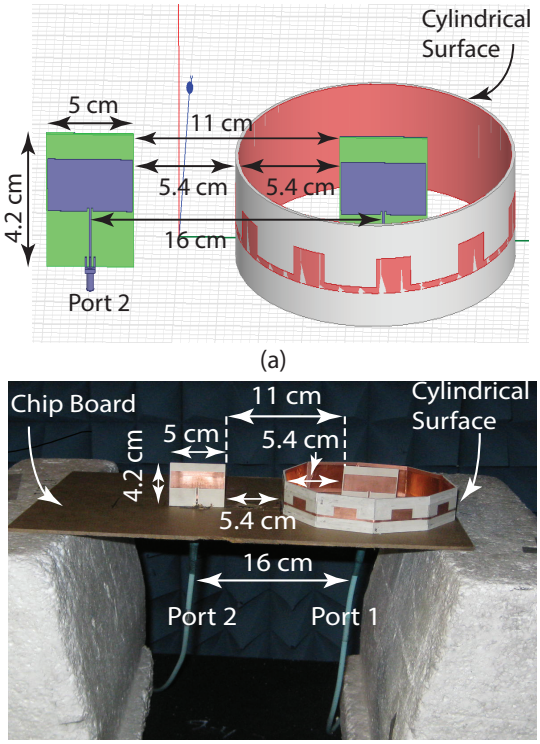

Figure 24. (a) HFSS simulation geometry of shielding an antenna surrounded by cylindrical surface from the EM waves of another antenna, both antennas are radiating at the operating frequency of the cylindrical surface i.e., 3.89 GHz (b) measurement set-up in the full anechoic chamber of shielding an antenna surrounded by the cylindrical surface from the EM waves of another antenna, both antennas are radiating at the operating frequency of the cylindrical surface i.e., 3.89 GHz.

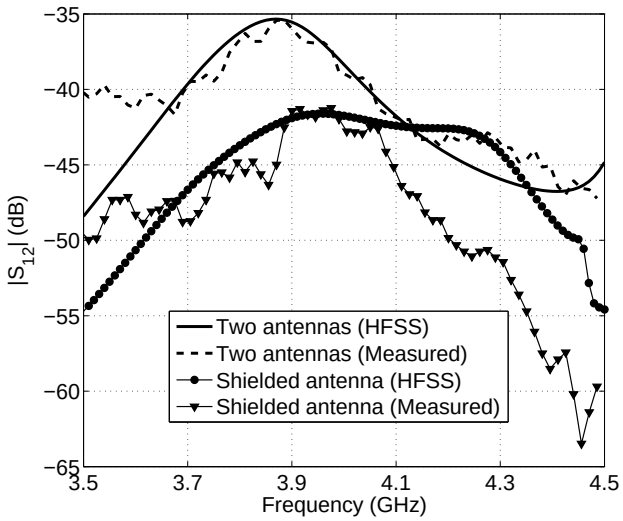

Figure 25. Measured and simulated S_{12} of the shielding cylindrical surface for the two microstrip patch antennas.

Next, the same microstrip patch antennas considered vertically in Fig. 23 were placed horizontally in a full anechoic chamber and $|S_{12}|$ was measured. The measurement is shown in Fig. 26(a). To validate the reduction in mutual coupling for horizontally placed antenna arrays, the antenna driven by port 1 (antenna on right in Fig. 26(a)) was surrounded by the cylindrical surface and the $|S_{12}|$ values were measured (as shown in Fig. 26(b)).

The results in Fig. 27 show that the $|S_{12}|$ values between the two horizontally placed microstrip patch antennas without the cylindrical surface in place are measured to be $-36.3\ dB$. Then, when the antenna fed with port 1 was shielded by the cylindrical surface, the measured $|S_{12}|$ values were reduced to -44.6 dB. The difference between the $|S_{12}|$ values of the horizontally placed microstrip patch antennas with and without the cylindrical surface are more than 8 dB. The shielding of horizontally placed antennas also validates the cylindrical surface similar to a cloaking-surface.

4.5. The Effect Of The Cylindrical Surface On The Radiation Pattern And Gain Of A 2-Element Array In Scattering Environments

To analyze the effects of a cylindrical surface on the radiation pattern of a two-antenna array, the gain of the 2-antennas with and without the cylindrical surface was measured. The antennas of dimensions shown in Fig. 23 and radiating at 3.89 GHz were used for the gain measurements. For the first step, antenna-1 was driven while antenna-2 was terminated with a matched load, as shown in Fig. 28(a), and the gain was measured. Then antenna-1 was surrounded by the cylindrical surface, as shown in Fig. 28(b), and the gain was measured. For the second step, to validate the effect of the cylindrical surface on the gain of the two antennas, antenna-2 was driven when antenna-1 was terminated with a matched load, as shown in Fig. 28(a), and the gain was measured. Then antenna-1 was surrounded by the cylindrical surface, as shown in Fig. 28(b) and the gain was measured. The resultant gains for all measurements

are shown in Table 1. Table 1 illustrates that the presence of the cylindrical surface has almost no effect on the gain of antenna-2.

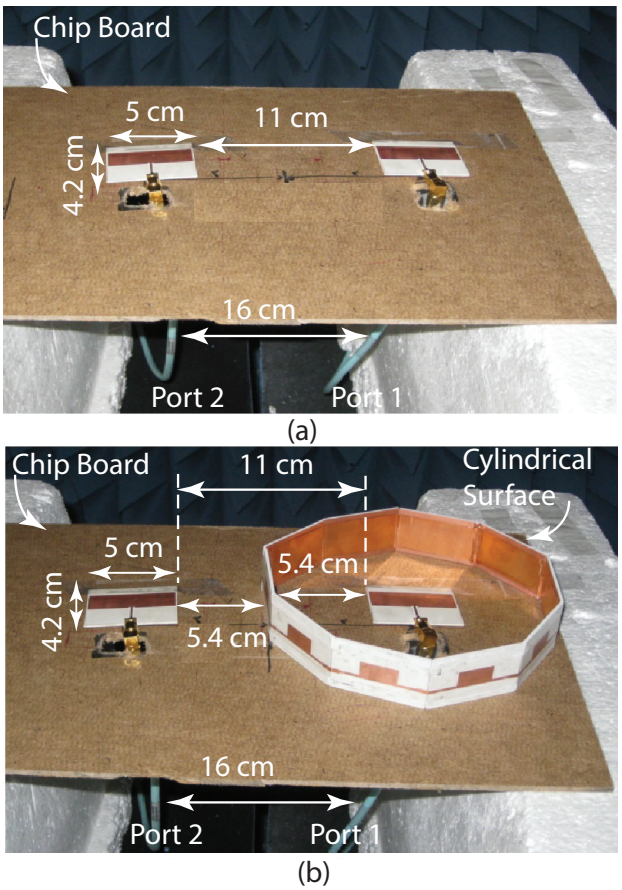

Figure 26. (a) Two horizontally placed microstrip patch antennas in a full anechoic chamber (b) One microstrip patch antenna surrounded by cylindrical surface in a full anechoic chamber .

Next the two antennas radiating at the frequency of 3.89 GHz were connected to a power splitter [58] to make a two-element array, as shown in Fig. 29(a), and the radiation pattern was measured in the full anechoic chamber. Next, one of the antennas (antenna-1) was enclosed in the cylindrical surface as shown in Fig. 29(b) and again, the radiation pattern for the two-element array was measured in the full anechoic chamber.

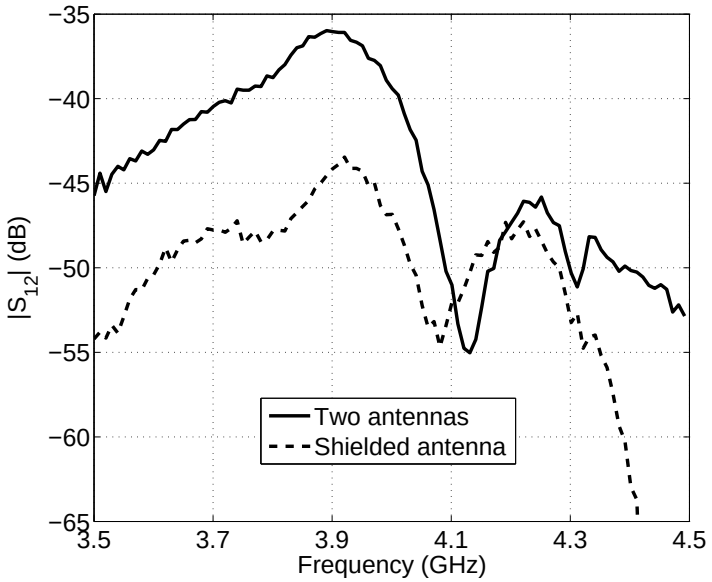

Figure 27. Measured S_{12} of the shielding cylindrical surface for the two horizontally placed microstrip patch antennas.

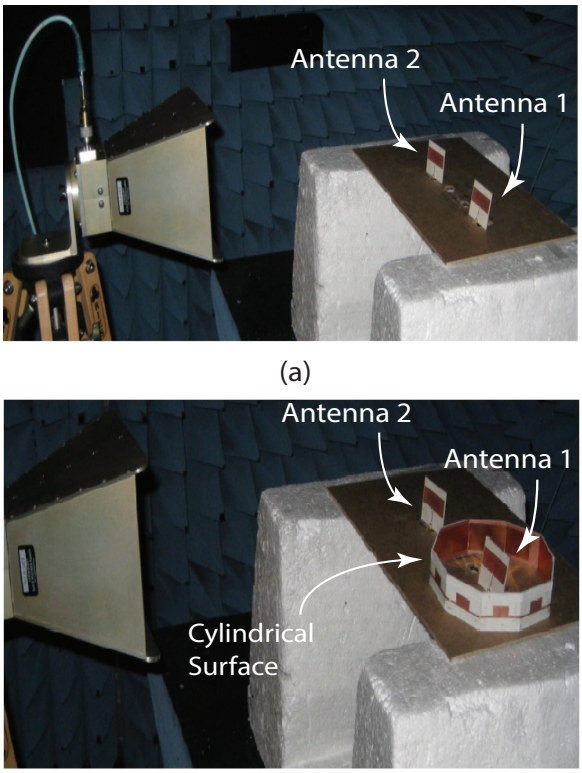

Figure 28. Gain measurement of the two microstrip patch antennas in a full anechoic chamber when antenna 1 is driven and antenna 2 is terminated with the match load (a) without cylindrical surface (b) antenna 1 is surrounded by cylindrical surface.

Table 1. Gain of flat antenna array.

	Antenna 1 is driven		Antenna 2 is driven	
	Without Cylindrical Surface	With Cylindrical Surface	Without Cylindrical Surface	With Cylindrical Surface
Gain (dB)	6.9	3.1	6.9	6.8

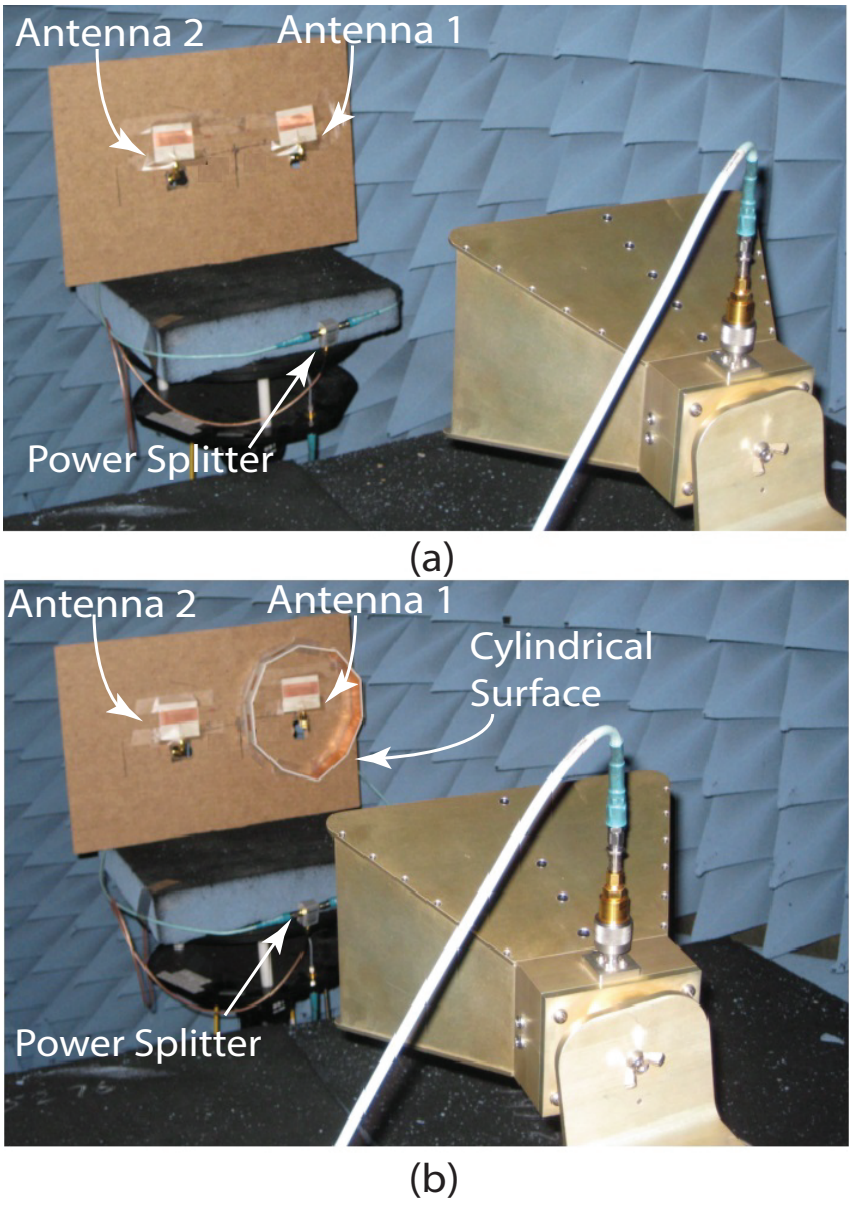

Figure 29. Pattern measurement of a two-antenna array in a full anechoic chamber (a) two-antenna array (b) One antenna is surrounded by cylindrical surface.

The polar plot and the rectangular plot for the array with and without the cylindrical surface are shown in Fig. 30 and Fig. 31 respectively, and are in good agreement, which shows that the cylindrical surface has negligible effects on the radiation pattern. Moreover, the gain of the two-element array with and without the cylindrical surface was measured to be 5.8 dB and 5.7 dB respectively. These results illustrate that the cylindrical surface has negligible effects on the far-field parameters of a two-element array and validates the functionality of the cylindrical surface.

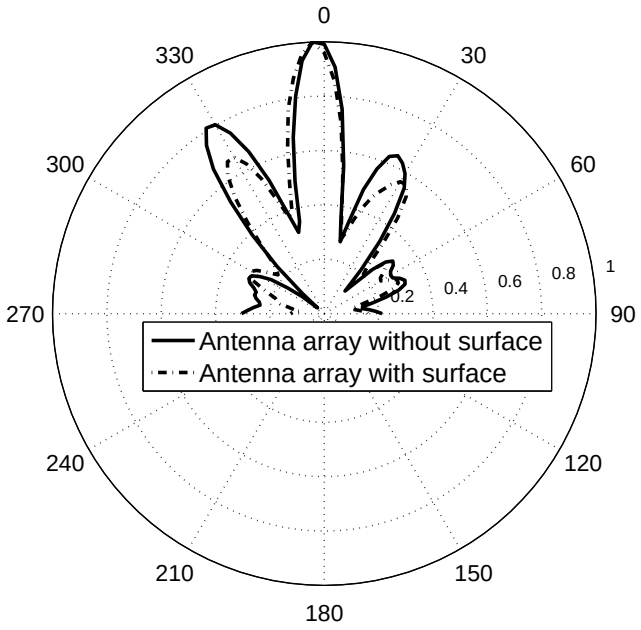

Figure 30. Polar plot of a two-antenna array with and without the cylindrical surface.

4.6. Discussion

The $|S_{12}|$ results presented in Fig. 25 and Fig. 27 show that the cylindrical surface has the capability to shield one antenna from the EM waves of the other by channeling the EM waves and thus reduce the mutual coupling between them. The results in Table 1 and Fig. 30 show that the presence of the cylindrical surface has no effect on the far field parameters, (i.e., gain and radiation pattern of an antenna

array). Thus demonstrates the application of a cylindrical surface with cloaking properties to an antenna array system.

In summary, it was shown that the designed cylindrical surface with cloaking properties can reduce the mutual coupling between two antennas more than 6 dB and has almost no effect on the radiation pattern and the gain of a two-element array. Thus, the cylindrical surface is capable of being use in antenna array applications.

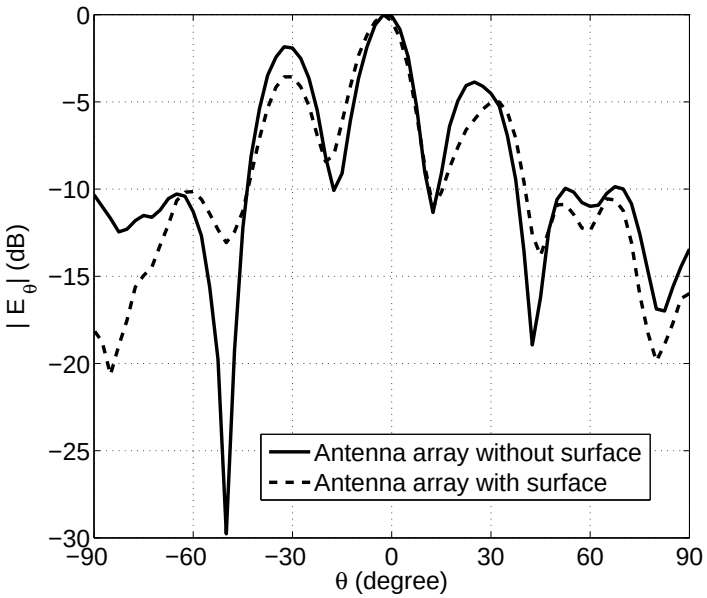

Figure 31. Rectangular plot of a two-antenna array with and without the cylindrical surface.

CHAPTER 5. CONCLUSION

In this work, a cylindrical surface exhibiting the properties of transformation-based and transmission-line based cloaks was used to shield an antenna array. Initially, a single-port frequency reconfigurable microstrip structure was designed and presented. Then, this single-port element was used to develop a two-port frequency reconfigurable element. The two-port frequency reconfigurable element has a larger and smaller conducting patch that loads a printed transmission line connecting ports 1 and 2. The frequency reconfigurable cylindrical-shape surface consisted of 10 interconnected two-port frequency reconfigurable elements. The simulation environment was described and a prototype was manufactured for validation. It was shown that the cylindrical surface is capable of reducing the scattering from a conducting cylinder in both frequency reconfigurable bands and achieving $|S_{12}|$ values within 1.3 dB of the values without the conducting cylinder in place.

To reduce the mutual coupling between two antennas radiating at 3.89 GHz, a cylindrical surface exhibiting the properties of an EM cloak at 3.89 GHz was designed next. The surface consisted of 10 interconnected two-port microstrip elements each with a conducting surface that loads a printed transmission line connecting ports 1 and 2. The capability of the cylindrical surface to reduce the scattering from a conducting cylinder was validated first in simulation and then by measurement. Then, the cylindrical surface was used to reduce the mutual coupling between two antennas, by surrounding one of them with the cylindrical surface. It was shown that the cylindrical surface can reduce the mutual coupling more than 6 dB and can be use as a shielding device for antenna arrays. Furthermore, it was shown that the cylindrical surface has a negligible effect on the far-field antenna array parameters by measuring the radiation pattern and gain of the two-element array.

Overall, simulations were validated with measurements and it was shown that 1) a cylindrical-shape surface with cloaking properties and minimal manufacturing difficulties as compared to traditional cloaking surfaces could be developed by using printed microstrip structures; 2) a frequency reconfigurable cylindrical surface with cloaking properties could be designed; 3) the cylindrical surface is compact enough to use for antenna applications instead of cloaking a traditional long conducting cylinder; and 4) the designed cylindrical surface was capable of being used in antenna array applications.

BIBLIOGRAPHY

[1] D. Schurig, J. J. Mock, B. J. Justice, S. A. Cummer, J. B. Pendry, A. F. Starr, and D. R. Smith, "Metamaterial electromagnetic cloak at microwave frequencies," *Science,* vol. 314, pp. 977-980, Nov. 2006.

[2] P. Alitalo and S. Tretyakov, "Electromagnetic cloaking with metamaterials," *Mater. Today,* vol. 12, pp. 22-29, Mar. 2009.

[3] J. B. Pendry, D. Schurig, and D. R. Smith, "Controlling electromagnetic fields," *Science,* vol. 312, pp. 1780-1782, Jun. 2006.

[4] U. Leonhardt, "Optical Conformal Mapping," *Science,* vol. 312, no. 5781, pp. 1777-1780, Jun. 2006.

[5] H. Chen, C. T. Chan, and P. Sheng, "Transformation optics and metamaterials," *Nat Mater,* vol. 9, no. 5, pp. 387-396, May 2010.

[6] B. Zhang, "Electrodynamics of transformation-based invisibility cloaking," *Light Sci Appl,* vol. 1, no. 10, p. e32, Oct. 2012.

[7] U. Leonhardt, "Notes on conformal invisibility devices," *New J. Phys.,* vol. 8, no. 7, p. 118, Jul. 2006.

[8] S. A. Cummer, B.-I. Popa, D. Schurig, D. R. Smith, and J. Pendry, "Full-wave simulations of electromagnetic cloaking structures," *Phys. Rev. E,* vol. 74, no. 3, p. 036621, Sep. 2006.

[9] F. Zolla, S. Guenneau, A. Nicolet, and J. B. Pendry, "Electromagnetic analysis of cylindrical invisibility cloaks and the mirage effect," *Opt. Lett.,* vol. 32, no. 9, pp. 1069-1071, May 2007.

[10] Z. Ruan, M. Yan, C. W. Neff, and M. Qiu, "Ideal Cylindrical Cloak: Perfect but Sensitive to Tiny Perturbations," *Phys. Rev. Lett.,* vol. 99, no. 11, p. 113903, Sep. 2007.

[11] H. Chen, B.-I. Wu, B. Zhang, and J. A. Kong, "Electromagnetic Wave Interactions with a Metamaterial Cloak," *Phys. Rev. Lett.,* vol. 99, no. 6, p. 063903, Aug. 2007.

[12] B. Zhang, H. Chen, B.-I. Wu, Y. Luo, L. Ran, and J. A. Kong, "Response of a cylindrical invisibility cloak to electromagnetic waves," *Phys. Rev. B,* vol. 76, no. 12, p. 121101, Sep. 2007.

[13] J. Perczel, T. Tyc, and U. Leonhardt, "Invisibility cloaking without superluminal propagation," *New J. Phys.,* vol. 13, no. 8, p. 083007, Aug. 2011.

[14] A. Sihvola, S. Tretyakov, and A. de Baas, "Metamaterials with extreme material parameters," *J. Commun. Technol. Electron.,* vol. 52, no. 9, pp. 986-990, Sep. 2007.

[15] D. Schurig, J. J. Mock, B. J. Justice, S. A. Cummer, J. B. Pendry, A. F. Starr, and D. R. Smith, "Metamaterial Electromagnetic Cloak at Microwave Frequencies," *Science,* vol. 314, no. 5801, pp. 977 980, Nov. 2006.

[16] U. Leonhardt and T. Tyc, "Broadband Invisibility by Non-Euclidean Cloaking," *Science,* vol. 323, no. 5910, pp. 110-112, Jan. 2009.

[17] J. Li and J. B. Pendry, "Hiding under the Carpet: A New Strategy for Cloaking," *Phys. Rev. Lett.,* vol. 101, no. 20, p. 203901, Nov. 2008.

[18] J. C. Halimeh, T. Ergin, J. Mueller, N. Stenger, and M. Wegener, "Photorealistic images of carpet cloaks," *Opt. Express,* vol. 17, no. 22, pp. 19328-19336, Oct. 2009.

[19] T. Ergin, J. C. Halimeh, N. Stenger, and M. Wegener, "Optical microscopy of 3D carpet cloaks: ray-tracing calculations," *Opt. Express,* vol. 18, no. 19, pp. 20535-20545, Sep. 2010.

[20] R. Liu, C. Ji, J. J. Mock, J. Y. Chin, T. J. Cui, and D. R. Smith, "Broadband Ground-Plane Cloak," *Science,* vol. 323, no. 5912, pp. 366-369, Jan. 2009.

[21] H. F. Ma and T. J. Cui, "Three-dimensional broadband ground-plane cloak made of metamaterials," *Nat. Commun,* vol. 1, p. 21, Jun. 2010.

[22] D. Shin, Y. Urzhumov, Y. Jung, G. Kang, S. Baek, M. Choi, H. Park, K. Kim, and D. R. Smith, "Broadband electromagnetic cloaking with smart metamaterials," *Nat. Commun,* vol. 3, p. 1213, Nov. 2012.

[23] B. Zhang, Y. Luo, X. Liu, and G. Barbastathis, "Macroscopic Invisibility Cloak for Visible Light," *Phys. Rev. Lett.,* vol. 106, no. 3, p. 033901, Jan. 2011.

[24] X. Chen, Y. Luo, J. Zhang, K. Jiang, J. B. Pendry, and S. Zhang, "Macroscopic invisibility cloaking of visible light," *Nat Commun,* vol. 2, p. 176, Feb. 2011.

[25] B. Wood and J. B. Pendry, "Metamaterials at zero frequency," *J. Phys.: Condens. Matter,* vol. 19, no. 7, p. 076208, Feb. 2007.

[26] Z. L. Mei, Y. S. Liu, F. Yang, and T. J. Cui, "A dc carpet cloak based on resistor networks," *Opt. Express,* vol. 20, no. 23, pp. 2575825765, Nov. 2012.

[27] J. Souc, M. Solovyov, F. Gmry, J. Prat-Camps, C. Navau, and A. Sanchez, "A quasistatic magnetic cloak," *New J. Phys.,* vol. 15, no. 5, p. 053019, May 2013.

[28] A. Alù and N. Engheta, "Plasmonic materials in transparency and cloaking problems: mechanism, robustness, and physical insights," *Opt. Express,* vol. 15, no. 6, pp. 3318-3332, Mar. 2007.

[29] A. Alù and N. Engheta, "Multifrequency Optical Invisibility Cloak with Layered Plasmonic Shells," *Phys. Rev. Lett.,* vol. 100, no. 11, p. 113901, Mar. 2008.

[30] A. Alù and N. Engheta, "Theory and potentials of multi-layered plasmonic covers for multi-frequency cloaking," *New J. Phys.,* vol. 10, no. 11, p. 115036, Nov. 2008.

[31] S. Tricarico, F. Bilotti, A. Al, and L. Vegni, "Plasmonic cloaking for irregular objects with anisotropic scattering properties," Phys. Rev. E, vol. 81, no. 2, p. 026602, Feb. 2010.

[32] A. Alù, "Mantle cloak: Invisibility induced by a surface," *Phys. Rev. B,* vol. 80, no. 24, p. 245115, Dec. 2009.

[33] P.-Y. Chen and A. Al, "Mantle cloaking using thin patterned metasurfaces," *Phys. Rev. B,* vol. 84, no. 20, p. 205110, Nov. 2011.

[34] P.-Y. Chen, F. Monticone, and A. Al, "Suppressing the Electromagnetic Scattering With an Helical Mantle Cloak," *IEEE Antennas and Wireless Propagation Letters,* vol. 10, pp. 1598-1601, 2011.

[35] J. C. Soric, P. Y. Chen, A. Kerkhoff, D. Rainwater, K. Melin, and A. Al, "Demonstration of an ultralow profile cloak for scattering suppression of a finitelength rod in free space," *New J. Phys.,* vol. 15, no. 3, p. 033037, Mar. 2013.

[36] B. Edwards, A. Alù, M. G. Silveirinha, and N. Engheta, "Experimental Verification of Plasmonic Cloaking at Microwave Frequencies with Metamaterials," *Phys. Rev. Lett.,* vol. 103, no. 15, p. 153901, Oct. 2009.

[37] D. Rainwater, A. Kerkhoff, K. Melin, J. C. Soric, G. Moreno, and A. Al, "Experimental verification of three-dimensional plasmonic cloaking in freespace," *New J. Phys.,* vol. 14, no. 1, p. 013054, Jan. 2012.

[38] P. Alitalo, O. Luukkonen, L. Jylha, J. Venermo, and S. A. Tretyakov, "Transmission-Line Networks Cloaking Objects From Electromagnetic Fields," *IEEE Transactions on Antennas and Propagation,* vol. 56, no. 2, pp. 416-424, 2008.

[39] G. Gok and A. Grbic, "Tensor Transmission-Line Metamaterials," *IEEE Transactions on Antennas and Propagation,* vol. 58, no. 5, pp. 1559-1566, 2010.

[40] J. Wang, S. Qu, Z. Xu, H. Ma, J. Zhang, Y. Li, and X. Wang, "Super-thin cloaks based on microwave networks," *IEEE Trans. on Antennas and Propaga.,*, vol. 61, No. 2, pp. 748-754, Feb. 2013.

[41] A. Naqvi and B. D. Braaten, "A two-port frequency reconfigurable microstrip element for conformal cloaking," *2014 IEEE International Symposium on Antennas and Propagation,* Jul. 6 - 12, 2014, Memphis, TN.

[42] S. Tretyakov, P. Alitalo, O. Luukkonen, and C. Simovski, "Broadband Electromagnetic Cloaking of Long Cylindrical Objects," *Phys. Rev. Lett.,* vol. 103, no. 10, p. 103905, Sep. 2009.

[43] P. Alitalo and S. A. Tretyakov, "Electromagnetic cloaking of strongly scattering cylindrical objects by a volumetric structure composed of conical metal plates," *Phys. Rev. B,* vol. 82, no. 24, p. 245111, Dec. 2010.

[44] P. Alitalo, A. E. Culhaoglu, A. V. Osipov, S. Thurner, E. Kemptner, and S. A. Tretyakov, "Bistatic scattering characterization of a three-dimensional broadband cloaking structure," *Journal of Applied Physics,* vol. 111, no. 3, pp. 034901-034901-5, 2012.

[45] A. Greenleaf, Y. Kurylev, M. Lassas, and G. Uhlmann, "Full-Wave Invisibility of Active Devices at All Frequencies," *Commun. Math. Phys.,* vol. 275, no. 3, pp. 749-789, Nov. 2007.

[46] F. G. Vasquez, G. W. Milton, and D. Onofrei, "Active Exterior Cloaking for the 2D Laplace and Helmholtz Equations," *Phys. Rev. Lett.,* vol. 103, no. 7, p. 073901, Aug. 2009.

[47] Q. Ma, Z. L. Mei, S. K. Zhu, T. Y. Jin, and T. J. Cui, "Experiments on Active Cloaking and Illusion for Laplace Equation," *Phys. Rev. Lett.,* vol. 111, no. 17, p. 173901, Oct. 2013.

[48] D.-H. Kwon and D. H. Werner, "Restoration of antenna parameters in scattering environments using electromagnetic cloaking," *Appl. Phys. Lett.,* vol. 92, no. 11, pp. 113507-113507-3, 2008.

[49] P. Alitalo, C. Valagiannopoulos, and S. A. Tretyakov, "Simple cloak for antenna blockage reduction," in *Proc. IEEE APS Int. Symp.,* 2011, pp. 669-672.

[50] P. Alitalo, J. Vehmas, and S. A. Tretyakov, "Reduction of antenna blockage with a transmission-line cloak," in *Proc. 5th EuCAP,* 2011, pp. 2399-2402.

[51] A. Monti , J. Soric , A. Alù , F. Bilotti , A. Toscano and L. Vegni "Overcoming mutual blockage between neighboring dipole antennasusing a low-profile patterned metasurface," *IEEEAntennas Wireless Propag. Lett.,* vol. 11, pp.1414 -1417, 2012.

[52] Advanced Design System-ADS 2004A Agilent Technologies.

[53] High Frequency Structure Simulator, HFSS 2009, Version 11.2, Ansoft, LLC.

[54] Skyworks Inc. [Online]. Available: www.skyworksinc.com

[55] Rogers Corporation [Online]. Available: www.rogerscorp.com

[56] C. A. balanis, "Antenna Theory Analysis and Design," *John Wiley and Sons,* 2005.

[57] D. N. West and S. K. Sharma, "Frequency Reconfigurable Compact Multiband Quasi-Log Periodic Dipole Array (QLPDA) Antenna for Wireless Communications", *IEEE Int. Symp. on Antennas and Propaga.* Toronto CA, July 11 - 17, 2010.

[58] Mini-Circuits Inc. [Online]. Available: www.minicircuits.com